Article

Mineralogy and chemistry of a new halloysite deposit from the Rio de Janeiro pegmatite province, south-eastern Brazil

Victor Matheus Joaquim Salgado-Campos[1,2]* [ID], Luiz Carlos Bertolino[2,3], Francisco José da Silva[4],

Julio Cezar Mendes[1] and Reiner Neumann[2,5]

[1]Federal University of Rio de Janeiro, Institute of Geosciences, Graduate Program in Geology, Athos da Silveira Ramos Avenue, 274 – Cidade Universitária, Rio de Janeiro – RJ, 21941-909, Brazil; [2]Centre for Mineral Technology, Division for Technological Characterization, Avenida Pedro Calmon, 900 – Cidade Universitária, Rio de Janeiro – RJ, 21941-908, Brazil; [3]State University of Rio de Janeiro, Faculty of Geology, Department of Mineralogy and Igneous Petrology, São Francisco Xavier Street, 524 – Maracanã, Rio de Janeiro – RJ, 20550-000, Brazil; [4]Federal Rural University of Rio de Janeiro, Institute of Agronomy, Department of Petrology and Geotectonics, BR 465 Highway, Km 07, s/n Zona Rural – Seropédica – RJ, 23890-000, Brazil and [5]Federal University of Rio de Janeiro, Graduate Program in Geosciences, National Museum, Av. Quinta da Boa Vista, S/N – Bairro Imperial de São Cristóvão, Rio de Janeiro – RJ, 20940-040, Brazil

Abstract

Halloysite is a 1:1 dioctahedral clay mineral that has been studied widely for applications in nanotechnology and as a mineral exploration guide for recognizing regolith-hosted heavy rare earth element (*HREE*) deposits. In Brazil, pegmatites from the state of Rio de Janeiro have been catalogued, but their potential to host halloysite deposits has never been studied. After a mineral exploration programme, one pegmatite with considerable halloysite contents and economic potential was discovered. This study reports the mineralogical and chemical characterization of the halloysite of this pegmatite and evaluates the possibility of clay-adsorbed *HREE* deposits, like that in the Zudong (China) regolith-hosted *HREE* deposit. Seven samples were collected in horizontal channels. Bulk samples and clay fractions (<2 µm) were analysed by quantitative mineral analysis (X-ray diffraction/Rietveld method), chemical analysis (major elements by X-ray fluorescence and Y, U, Th and rare earth elements by inductively coupled plasma mass spectrometry), scanning electron microscopy, Fourier-transform infrared spectroscopy, particle-size analysis, nitrogen physisorption and cation-exchange capacity. Mixed polygonal/cylindrical halloysite-7Å in concentrations between 6.3 and 35.4 wt.% in bulk samples and between 58.0 and 89.8 wt.% in the clay fractions were identified in the pegmatite. The clay fractions presented an average chemical composition of 45.46 wt.% SiO_2, 36.10 wt.% Al_2O_3, 14.62 wt.% loss on ignition and 1.04 wt.% Fe_2O_3, as well as technological properties close to those observed in world-class halloysite deposits such as Dragon Mine (USA) and Matauri Bay (New Zealand). The clay minerals did not present significant *HREE* contents.

Keywords: Brazil, clay mineralogy, halloysite, nanosciences, nanotechnology, pegmatite, regolith, Rio de Janeiro

Halloysite is a 1:1 dioctahedral clay mineral and a polytype of kaolinite (Guggenheim *et al.*, 2006; Drits *et al.*, 2018). One of the main characteristics that differentiates halloysite from kaolinite is its tubular morphology (Velde & Meunier, 2008). This feature improves significantly its technological properties, resulting in a greater surface area and the presence of a lumen. The tubular morphology can be classified as polygonal or cylindrical, the latter having improved technological characteristics, but both types have been used in industry (Hillier *et al.*, 2016).

Because of its tubular morphology and natural origin, halloysite (or halloysite nanotubes (HNTs)) is more cost-effective and environmentally friendly than artificial nanotubes (e.g. of carbon). Since 2005, studies of the applications of halloysite have increased exponentially with an emphasis on the pharmaceutical

sector, in which the mineral has been used and studied as an active agent carrier (Churchman *et al.*, 2016). The mineral also gained attention recently due to the presence of heavy rare earth elements (*HREEs*) in its lumen, giving rise to regolith-hosted *HREE* deposits (Li *et al.*, 2019; Li & Zhou, 2020).

The mineral is composed of a tetrahedral sheet of $Si^{4+}O_4$, where Si can be replaced by Al^{3+} in minor proportions, an octahedral sheet of oxygen-surrounded Al^{3+} that can be replaced by Fe^{3+} or Fe^{2+} and an interlayer region with water molecules (Joussein *et al.*, 2005). Theoretically, Ti^{4+} could also replace Al^{3+} in the octahedral sheet, but Weaver (1976) showed that this cation is associated with nanocrystals of rutile. The hydration state of the interlayer allows us to classify halloysite as halloysite-7Å $(Al_2Si_2O_5(OH)_4)$, a fully dehydrated state of halloysite, or halloysite-10Å $(Al_2Si_2O_5(OH)_4.2H_2O)$, which represents a fully hydrated state of halloysite.

Halloysite deposits around the world are formed mostly by hydrothermal alteration, but also by weathering processes, and not by sedimentary processes, which generate kaolinite-type deposits (Prasad *et al.*, 1991; Wilson & Keeling, 2016).
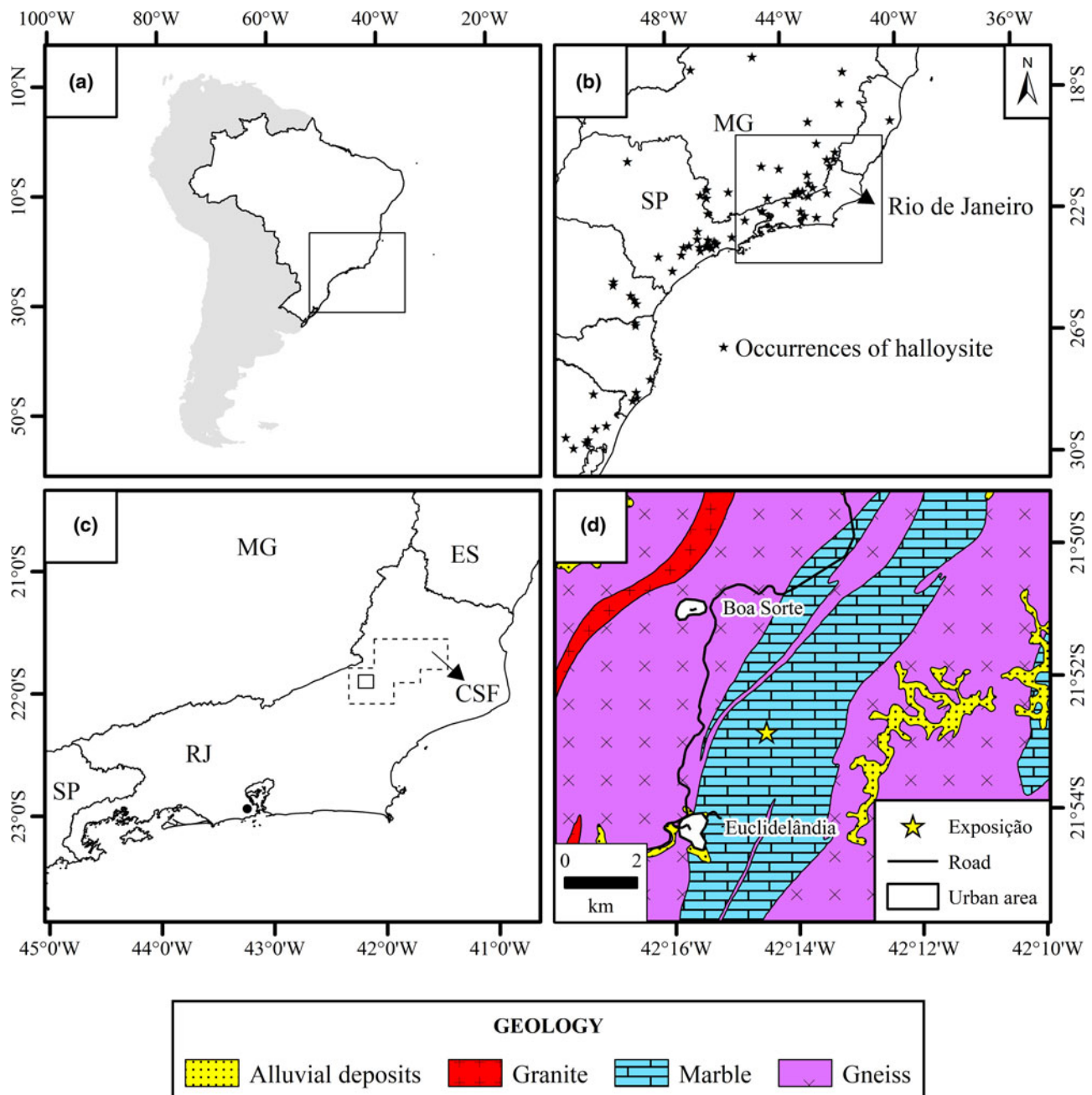
Fig. 1. Location of the Exposição pegmatite. (a) Location of the Exposição pegmatite in South America. (b) Compilation of deposits and halloysite occurrences in the south and south-east regions of Brazil (based on Paiva *et al.*, 1956; Visconti & Nicot, 1956, 1957; Souza Santos *et al.*, 1962, 1964, 2009; Angeleri *et al.*, 1963; Pimentel, 1966; Souza Santos & Pimentel, 1971; Azevedo & Souza Santos, 1975; Campos & Souza Santos, 1986; Wilson *et al.*, 1998, 2006; Toledo *et al.*, 2002; Oliveira *et al.*, 1997, 2007; Santos, 2017; Tolentino, 2019). (c) Location of the Cantagalo-São Fidélis (CSF) area, represented by a polygon, in the Rio de Janeiro Pegmatite Province (modified from Menezes, 1997). (d) Geological map (modified from Heilbron *et al.*, 2016) of the region showing the location of the Exposição pegmatite (21°52′56′′S; 42°14′36′′W). ES = Espírito Santo; MG = Minas Gerais; RJ = Rio de Janeiro; SP = São Paulo.

The main world-class halloysite deposits are at Dragon Mine (USA) (Kildale & Thomas, 1957; Morris, 1964, 1985), Matauri Bay (New Zealand) (Brathwaite *et al.*, 2012), Guizhou, Yunnan and Hunan provinces (China) (Wilson, 2004) and Biga Peninsula (Turkey) (Ece *et al.*, 2008).

Kaolin deposits hosted by pegmatites around the world include the Bombowha deposit (Ethiopia) (Fentaw & Mengistu, 1998), Hagendorf Pleystein Pegmatite Province (Germany) (Dill *et al.*, 2015), Swat deposits (Pakistan) (Saddiqui & Ahmed, 2005) and the Spruce Pine deposit in the USA (Parker, 1946). Halloysite

occurs only in the Bombowha and Swat deposits, where it is mixed with kaolinite.

In Brazil, the occurrence of halloysite appears to be restricted to the south-eastern and southern regions of the country. In the north and northeast, no halloysite was detected in the kaolin sedimentary deposits of Capim River (Sousa *et al.*, 2007) or Jari River (Montes *et al.*, 2002), nor in the Borborema Pegmatite Province (Salgado-Campos *et al.*, 2017, 2019). The occurrences of halloysite in southern and south-eastern Brazil include those of the states of Minas Gerais (Tolentino, 2019), Espírito Santo (Wilson

Fig. 2. Channel sampling sites located along the face of the pegmatite. (a) Overview of the outcrop of Exposição pegmatite. (b) Overview of the right part of the outcrop with the location of horizontal channels, where the samples A, B and C were collected. (c) The right part of the outcrop, where sample A was collected in a 4 m-long channel. (d) Sampling location of sample B in a channel 4.2 m long. (e) The left part of the outcrop, where sample D was collected in a horizontal channel 2 m long. (f) Detail of the left part of the outcrop. (g) Sampling location of sample F on the left part of the outcrop. (h & i) Close views of the segments where samples G and F were collected in horizontal 2.0 and 2.5 m channels, respectively. (j) Details of the kaolin occurrence in the pegmatite.

et al., 2006), São Paulo (Wilson et al., 1998), Paraná (Oliveira et al., 2007), Santa Catarina (Wilson et al., 1998), Rio Grande do Sul (Wilson et al., 2006) and Rio de Janeiro. In the state of Rio de Janeiro, halloysite was found in the cities of Magé, Valença (Visconti & Nicot, 1956), Sapucaia, Petrópolis (Visconti & Nicot, 1957), Itatiaia, Araruama (Souza Santos et al., 1962), Rio Bonito (Santos, 2017; Salgado-Campos et al., 2020) and in the city of Rio de Janeiro (Souza Santos &

Table 1. Ranges of values used in this work to classify the Pearson correlation coefficients.

ρ value (+ or –)	Interpretation
0.00–0.19	Very weak correlation
0.20–0.39	Weak correlation
0.40–0.69	Moderate correlation
0.70–0.89	Strong correlation
0.90–1.00	Very strong correlation
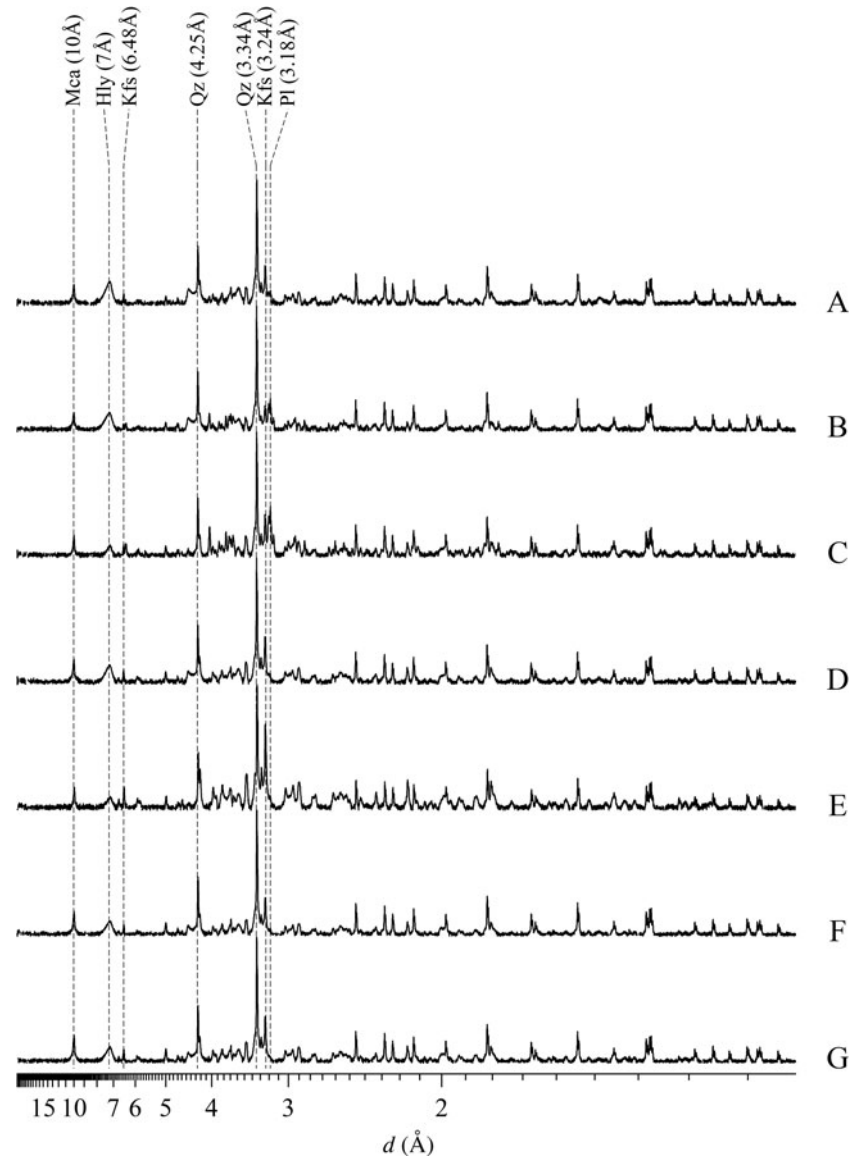
Fig. 3. XRD traces (background subtracted) of the bulk samples used in the quantitative mineral analyses by Rietveld refinement. The y-axis is on the square root scale and the diffraction traces were normalized by maximum reflection. The unprocessed data can be found in the Supplementary Materials. Hly = halloysite-7Å; Kfs = K-feldspar; Mi = mica; Pl = plagioclase; Qz = quartz.
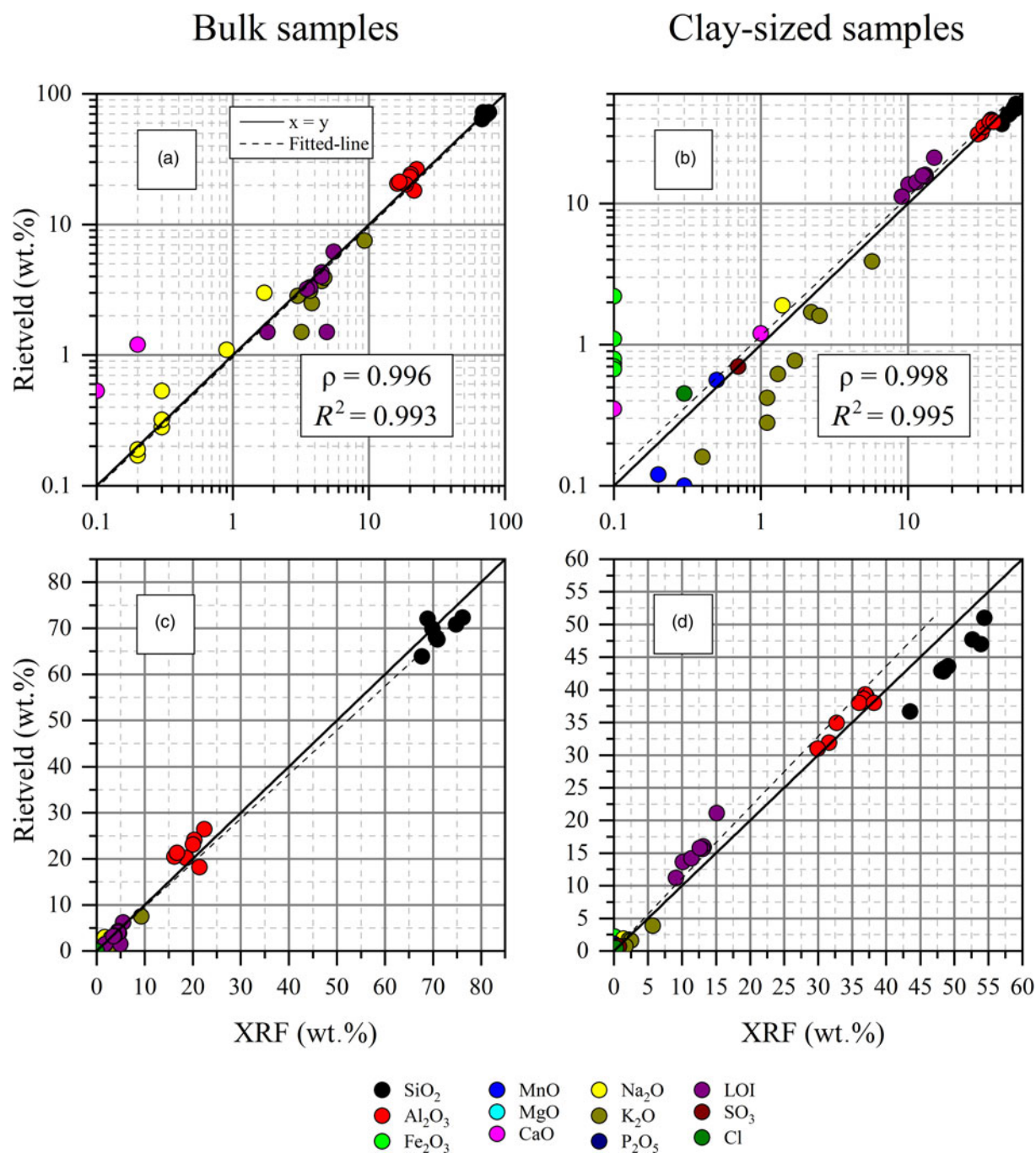
Table 2. Quantitative mineral and chemical analyses of the bulk samples. See refinement reports and Table S1 in the Supplementary Materials for more details.

	A	B	C	D	E	F	G
Mineralogy							
Dioctahedal mica	15.0	18.2	9.4	13.2	21.4	9.9	10.5
Halloysite-7Å	35.4	26.8	32.3	28.4	6.3	23.8	22.0
Quartz	35.2	41.0	32.5	38.4	29.5	50.1	45.7
K-feldspar	11.8	6.4	11.0	17.7	40.2	14.8	20.4
Plagioclase	2.4	7.6	14.8	2.3	2.6	1.4	1.4
Total	100.0	100.0	100.0	100.0	100.1	100.0	99.9
Chemical assay							
SiO_2	63.90	67.60	72.10	68.10	69.90	72.30	70.80
Al_2O_3	26.40	24.10	18.20	23.10	20.20	20.50	21.30
Fe_2O_3	0.56	0.65	0.88	0.69	0.32	0.53	0.41
MnO	0.05	0.05	0.14	0.05	0.05	0.05	0.05
MgO	0.12	0.11	0.10	0.14	0.05	0.10	0.10
CaO	0.10	0.53	1.20	0.05	0.05	0.05	0.05
Na_2O	0.28	1.10	3.00	0.32	0.53	0.17	0.19
K_2O	2.50	1.50	2.84	3.70	7.50	3.10	3.90
LOI	6.20	4.30	1.50	4.00	1.50	3.30	3.20
Total	100.11	99.94	99.96	100.15	100.10	100.10	100.00

Pimentel, 1971) (Fig. 1a,b). However, the lack of detailed geological and evaluation studies concerning the occurrences of halloysite in the state has meant that the real potential of Rio de Janeiro in hosting this type of halloysite deposit remains unknown. Thus, a systematic mineral exploration study was conducted on the aforementioned occurrences and a few were found to be feasible halloysite deposits (Salgado-Campos *et al.*, 2020). Nevertheless, a new pegmatite body that meets the size and halloysite-grade requirements may have economic potential, and its description is the primary objective of the present report.

Geological context

The pegmatite studied here, referred to as Exposição, is in the Rio de Janeiro Pegmatite Province (Menezes, 1982, 1997), Cantagalo-São Fidélis area. Four additional areas in the Pegmatite Province were included: Niterói-Rio Bonito, Paraíba do Sul, Casemiro de Abreu-Glicério and Barra Mansa-Barra do Piraí (Fig. 1c,d). The Cantagalo-São Fidélis area covers ~3300 km², where 33 pegmatites were catalogued by Menezes (1982),

Bulk samples

Clay-sized samples

Fig. 4. Correlation diagrams showing the chemical compositions calculated from quantitative mineral analyses using the Rietveld method against chemical assays by X-ray fluorescence (XRF). Assumed mineral compositions may be found in Tables S1 and S2. (a) Square root-scale graph of the bulk samples. (b) Square root-scale graph of the clay fractions. (c) Linear-scale graph of the bulk samples. (d) Linear-scale graph of the clay fractions.

although this did not include the one described here. The Exposição pegmatite is exposed in an outcrop that is ~60 m long, 10 m high and with an undetermined width. The pegmatite was classified as a mixed pegmatite following Silva & Dantas (1997) because of the presence of dispersed cm-sized mica zones, its graphic texture and the widespread garnet crystals.

Materials and methods

Seven channel samples with lengths between 2.0 and 4.2 m were collected from the newly discovered Exposição pegmatite (Fig. 2).

A standard halloysite sample from Sigma-Aldrich (685445-100G/ Chemical Abstracts Service (CAS) Number 1332-58-7) was analysed for comparative purposes.

The samples were dried at 60°C for 24 h before jaw crushing at 2 mm followed by homogenization and quartering in aliquots of 1 kg. Smaller aliquots were processed cyclically for bulk samples in a vibratory agate ring mill for 30 s at 700 rpm to obtain fractions of <106 μm, which were then processed in a McCrone agate mill for 10 min using water to obtain <10 μm bulk fractions for quantitative mineral and chemical analyses. Aliquots of 1 kg were wet-sieved at 20 μm before the separation of the clay

Table 3. *REEs*, U and Th analysis (ppm) of the bulk fractions of the Exposição pegmatite.

REE	A	B	C	D	E	F	G	Standard
La	5.4	7.2	16.3	8.1	5.7	2.6	2.4	8.1
Ce	14.9	16.2	29.4	22.6	10.7	3.7	3.3	8.9
Pr	0.94	1.45	4.03	1.61	1.00	0.35	0.29	1.82
Nd	4.7	6.5	17.3	7.1	4.6	2.3	1.8	11.9
Sm	1.2	1.8	4.4	1.6	1.1	0.7	0.6	6.1
Eu	0.37	0.42	0.63	0.42	0.62	0.30	0.30	3.17
Gd	1.30	2.11	4.92	1.87	1.28	0.90	0.87	18.09
Tb	0.22	0.35	0.87	0.30	0.22	0.15	0.16	2.80
Dy	1.62	2.98	8.85	2.41	1.81	1.36	1.38	18.88
Ho	0.37	0.70	2.34	0.61	0.51	0.34	0.35	3.24
Er	1.46	3.06	10.22	2.45	2.05	1.26	1.40	9.02
Tm	0.23	0.47	1.66	0.40	0.33	0.20	0.20	0.99
Yb	1.8	3.9	13.6	3.1	2.6	1.6	1.6	5.5
Lu	0.28	0.59	2.13	0.50	0.39	0.25	0.24	0.63
Y	9.54	19.24	59.12	15.93	12.55	9.24	9.76	95.27
U	4.60	10.33	18.96	8.59	1.82	2.82	2.51	2.15
Th	6.5	9.8	22.0	12.9	6.4	5.0	3.4	2.4
ΣLREE	28.81	33.15	71.43	41.01	23.10	9.65	8.39	36.82
ΣHREE	16.82	33.40	103.71	27.57	21.74	15.30	15.96	154.42
ΣREE	45.63	66.55	175.14	68.58	44.84	24.95	24.35	191.24

fractions (<2 μm) using Stokes' law (Moore & Reynolds, 1989). The use of an ultrasonic bath and the addition of sodium hexametaphosphate (3 mg g^{-1}) to clay–water suspensions ensured adequate dispersion.

The mineralogy of the bulk and clay fractions was quantified using the Rietveld method and the fundamental parameters approach (Cheary & Coelho, 1992). Diffraction patterns were obtained with Bruker-AXS D4 Endeavor equipment, using filtered Co-*K*α (λ = 1.79021 Å) radiation operated at 40 kV and 40 mA with a step size of 0.01°2θ and a cumulative acquisition time of 184 s step^{-1} with a LynxEye position-sensitive detector in the range from 4 to 105°2θ. The quantitative mineral analysis was performed using the Bruker-AXS *TOPAS* v5 software, sourcing structures from the International Centre for Diffraction Data (ICDD) database (2019) and the Crystallography Open Database (COD). The mineral structures used were montmorillonite (COD 900277; Viani *et al.*, 2002), muscovite (ICDD 04-015-8226; Brigatti *et al.*, 2008), kaolinite (ICDD 00-014-0164 BISH; Goodyear & Duffin, 1961), quartz (ICDD 00-046-1045; Kern & Eysel, 1993), microcline (ICDD 00-019-0926; Technisch Physische Dienst, 1966), albite (ICDD 00-019-1184; Technisch Physische Dienst, 1967), calcite (modified; Santos *et al.*, 2017), dolomite (modified; Santos *et al.*, 2017) and alunite (COD 9012350; Schukow *et al.*, 1999). The abbreviations for the names of rock-forming minerals were based on Whitney & Evans (2010) and Warr (2020). Detailed information regarding the refinement parameters may be found in the Supplementary Materials.

Oriented samples on glass slides were produced following Moore & Reynolds (1989) to characterize the clay mineral assemblages. The slides were measured in the air-dried state, following ethylene glycol solvation for 16 h and after heating at 550°C for 2 h. Diffraction patterns were obtained using a Bruker-AXS D8 Advance ECO diffractometer with a LynxEye XE energy-discriminant position-sensitive detector and unfiltered Cu-*K*α radiation (λ = 1.5406 Å) operated at 40 kV and 25 mA with a step size of 0.01°2θ and a cumulative acquisition time of 92 s step^{-1}. A dynamic beam optimization (DBO) device was used.

Random mounted samples were produced by backloading and analysed in the Bruker-AXS D8 Advance ECO equipment with a step size of 0.02°2θ and a cumulative acquisition time of 92 s step^{-1} between 4 and 70°2θ, which was used to determine the 060 reflections. The type of tubular halloysite morphology was assessed using the cylindrical–polygonal (CP) index proposed by Hillier *et al.* (2016), analysing the region between 2.2 and 2.7 Å.

Chemical analyses were carried out by X-ray fluorescence spectrometry using a PanAnalytical Axios Max spectrometer. Samples were prepared in a VANEOX press with a 30 mm-diameter mould and a pressure of 20 tons for 30 s using boric acid (0.5 g g^{-1}) as a binder. Rare earth elements (*REEs*) Y, Th and U were analysed using inductively coupled plasma mass spectrometry (ICP-MS) following the lithium metaborate fusion method (IMS95R) at the SGS Geosol Laboratories LTDA in Brazil.

A Pearson correlation matrix was constructed using the mineralogical, chemical and technological data (Table S3). The obtained values were classified following Table 1.

Scanning electron microscopy was performed on a Quanta 250 field emission gun scanning electron microscope at the Military Institute of Engineering at an accelerating voltage of 25 kV. The samples were silver sputtered before analysis.

Fourier-transform infrared (FTIR) spectra were obtained using a Nicolet 6700 spectrometer at the Institute of Chemistry of the Federal University of Rio de Janeiro. The equipment has a diffuse reflectance accessory and spectra were obtained in the range from 4000 to 400 cm^{-1} through co-addition of 64 scans with a resolution of 4 cm^{-1}. Pellets were prepared with 1% of the sample and 99% of KBr.

Particle-size analysis was carried out on the clay fractions using a Malvern Mastersizer 2000 instrument. Suspensions with 30 mL of distilled water (with 3 mg g^{-1} sodium hexametaphosphate) and 0.5 g of clay-sized samples were prepared by ultrasonication. Nitrogen physisorption analyses were performed using a Micromeritics TriStar II PLUS instrument at –196°C (77K). The samples were pre-treated in a Micromeritics VacPrep 061 instrument at 120°C under vacuum (10^{-6} mmHg) for 24 h. The isotherms were obtained with 50 points performed during adsorption and desorption. Specific surface areas were calculated using the Brunauer–Emmett–Teller (BET) method (Brunauer *et al.*, 1938) and porosity graphs were obtained following the Barrett–Joyner–Halenda (BJH) method (Barrett *et al.*, 1951). Cation-exchange capacity (CEC) values were obtained using the methylene blue method described by ASTM C837-09 (2009).

Results

Bulk mineralogy

Quantitative mineral analysis (X-ray diffraction/Rietveld method)
Dioctahedral mica was determined by diagnostic reflections at 10 Å (001) and 5 Å (002), and its abundance ranged from 9.4% (sample F) to 21.4% (sample E). Diagnostic reflections of kaolin minerals were close to 7.00 Å (001) and 3.56 Å (002), amounting to between 6.3% (sample E) and 35.4% (sample A). Quartz was identified by reflections at 4.25 and 3.34 Å varying from 29.5% (sample E) to 50.1% (sample F). K-feldspar was identified by reflections at 6.48 and 3.24 Å, ranging from 6.4% (sample B) to 40.2% (sample E), and plagioclase was identified by reflections at 3.18 Å varying from 1.4% (samples F and G) to 14.8% (sample C) (Fig. 3, Table 2).
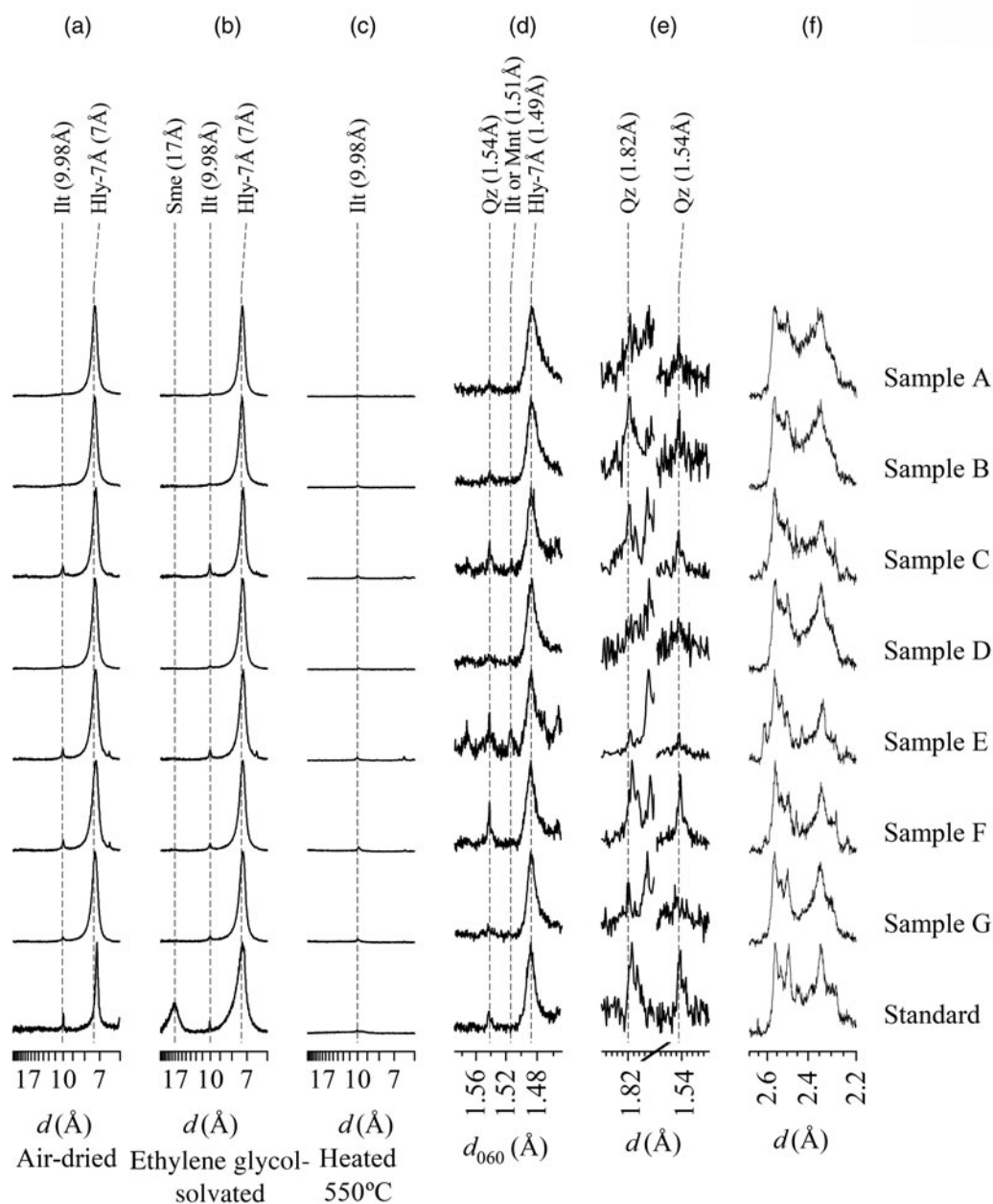
Fig. 5. XRD traces (background subtracted) of the oriented clay fractions mounted on glass slides. The unprocessed data can be found in the Supplementary Materials. (a) Air-dried oriented samples normalized by maximum intensity. (b) Ethylene glycol-solvated oriented samples with diffraction traces normalized by maximum intensity. (c) Oriented sample heated at 550°C normalized by maximum intensity of the air-dried oriented samples. (d) Randomly mounted samples in the region from 1.59 to 1.45 Å to evaluate the d_{060} reflections with diffraction patterns normalized by maximum intensity. (e) Randomly mounted samples to evaluate whether the d_{060} reflections at 1.54 Å are associated with quartz or another trioctahedral clay mineral, following Moore & Reynolds (1989), with diffraction traces normalized by maximum intensity. (f) Randomly mounted samples to assess the tubular character of halloysite (Hillier et al., 2016), with diffraction traces normalized by maximum intensity. Ilt = illite; Hly-7Å = halloysite-7Å; Mnt = montmorillonite; Qz = quartz; Sme = smectite.

Major elements by X-ray fluorescence

Chemical compositions calculated from quantitative mineral analyses were compared to chemical assays by X-ray fluorescence to evaluate the quality of the mineral quantification using the Rietveld method. Taking all samples together, the Pearson correlation index was 0.996, while R^2 reached 0.993 (Fig. 4). However, it is appropriate to acknowledge uncertainties concerning the SiO_2 and Al_2O_3 contents.

Major element values of the bulk samples are listed in Table 2. The Pearson correlation matrix (Table S3) shows that halloysite-7Å presented a strong positive correlation with MgO (0.83) and loss on ignition (LOI; 0.73) and a strong negative correlation with

SiO_2 (–0.71). K-feldspar abundance has a very strong correlation with K_2O (0.99) and a strong negative correlation with MgO (–0.74), whereas plagioclase content showed very strong positive correlations with CaO (1.00), Na_2O (0.99) and MnO (0.90) and a strong positive correlation with Fe_2O_3 (0.81).

Rare earth elements

The *REE* contents of the bulk samples are listed in Table 3, in which the Σ*HREE* contents are higher than the Σ*LREE* contents in samples B, C, F and G and the Sigma standard. The *REE* abundance (Σ*REE*) showed a very strong positive correlation with

Table 4. Quantitative mineral and chemical analyses (wt.%) of the clay fractions. See refinement reports and Table S2 in the Supplementary Materials for more details.

	A	B	C	D	E	F	G	S
Mineralogy								
Montmorillonite	0.0	0.0	0.0	0.0	0.0	0.0	0.0	1.0
Illite	5.4	5.4	7.6	5.4	8.6	8.7	6.0	4.1
Halloysite-7Å	89.8	89.3	65.5	88.3	58.0	73.9	85.3	83.8
Gibbsite	0.0	0.0	0.0	0.0	0.0	0.0	0.0	5.9
Quartz	0.7	1.3	4.2	1.2	3.3	6.5	1.5	1.8
K-feldspar	4.2	4.0	9.8	5.2	30.1	11.0	7.3	0.0
Plagioclase	0.0	0.0	12.9	0.0	0.0	0.0	0.0	0.0
Calcite	0.0	0.0	0.0	0.0	0.0	0.0	0.0	0.9
Dolomite	0.0	0.0	0.0	0.0	0.0	0.0	0.0	1.5
Alunite	0.0	0.0	0.0	0.0	0.0	0.0	0.0	0.9
Total	100.0	100.0	100.0	100.0	100.0	100.0	100.0	100.0
CP index	0.35	0.31	0.23	0.27	0.16	0.20	0.21	0.27
Chemical assay								
SiO_2	42.90	42.80	47.00	43.20	51.00	47.70	43.60	36.70
Al_2O_3	39.00	39.30	31.90	38.60	31.00	34.90	38.00	38.00
Fe_2O_3	0.74	0.67	2.20	1.10	1.10	0.79	0.70	0.67
MgO	0.05	0.05	0.00	0.05	0.10	0.10	0.12	0.56
CaO	0.15	0.14	0.35	0.11	0.12	0.08	0.18	1.20
Na_2O	0.37	0.45	1.90	0.32	0.74	0.37	0.39	0.52
K_2O	0.42	0.28	1.70	0.62	3.90	1.60	0.77	0.16
P_2O_5	0.42	0.45	1.10	0.45	0.77	0.40	0.44	0.05
LOI	15.90	16.00	13.62	15.60	11.20	14.20	15.80	21.10
Cl	0.00	0.00	0.00	0.00	0.00	0.00	0.00	0.70
SO_3	0.14	0.10	0.00	0.05	0.05	0.05	0.00	0.45
Total	100.09	100.24	99.87	100.10	99.98	100.19	100.00	100.11

plagioclase (0.93), while only Eu presented a strong positive correlation with the total feldspar content (0.82) (Table S3). In addition, it is well known that the main *REE* carriers are phosphate minerals, which were not determined in the bulk mineralogy of the samples because these minerals are generally accessories. Concerning the major elements, ΣREE showed very strong positive correlations with Na_2O (0.94) and CaO (0.91) and a strong positive correlation with Fe_2O_3 (0.85).

Clay mineralogy

Clay mineral assemblages
Halloysite-7Å was identified by reflections at 7.26 Å, which did not change after treatment with ethylene glycol and collapsed after heating at 550°C (Fig. 5a,b,c). Illite was determined by reflections at 10 Å, which changed neither after ethylene glycol solvation nor after heating at 550°C. Smectite was only identified in the Sigma standard sample by a reflection at 17 Å after ethylene glycol treatment (Brindley & Brown, 1980).

The halloysite-7Å phase has a reflection at 1.49 Å, representing the 060 reflections, whereas illite and smectite have reflections at 1.50 Å, suggesting that montmorillonite is the smectite species (Fig. 5d). The 1.54 Å reflection is attributed to quartz, which has a similar intensity to that of the 1.82 Å quartz reflection (Fig. 5e) (Moore & Reynolds, 1989).

The region between 2.2 and 2.7 Å could be used to classify the type of tubular halloysite (Hillier *et al.*, 2016) (Fig. 5f). The CP values ranged from 0.16 to 0.35, indicating mixed polygonal/cylindrical halloysite crystals (Table 4) (Hillier *et al.*, 2016). The formamide method was not effective because of the dehydrated state of halloysite-7Å (Churchman *et al.*, 1984).

Quantitative mineral analysis (X-ray diffraction/Rietveld method)
Concerning the quantitative mineral analysis of the <2 μm fractions, values from 58.0% (sample E) to 89.8% (sample A) were obtained for halloysite-7Å, from 5.4% (samples A and B) to 8.7% (F) for illite, from 0.7% (sample A) to 6.5% (sample F) for quartz and from 4.0% (sample B) to 30.1% (sample E) for K-feldspar (Fig. 6, Table 4). Plagioclase was only identified in sample C at 12.9%. For the Sigma standard, 1.0% montmorillonite, 4.1% illite, 83.8% halloysite-7Å, 5.9% gibbsite, 1.8% quartz, 0.9% calcite, 1.5% dolomite and 0.9% alunite were quantified.

Major elements by X-ray fluorescence
The Pearson correlation index was 0.998, whereas the R^2 index was 0.995 when the calculations included all of the samples (Fig. 4), despite some uncertainties concerning the accuracy of SiO_2 and Al_2O_3 measurements. The chemical analyses (major elements) of the clay fractions are listed in Table 4. Using the Pearson correlation matrix (Table S3), illite showed a very strong positive correlation with SiO_2 (0.95) and a strong negative correlation with Al_2O_3 (−0.89). In contrast, the halloysite-7Å abundance displays a very strong positive correlation with Al_2O_3 (0.99), a strong positive correlation with LOI values (0.96), very strong negative correlations with K_2O (−0.93) and SiO_2 (−0.96) and a strong negative correlation with P_2O_5 (−0.75). K-feldspar has very strong positive correlations with K_2O (0.98) and SiO_2 (0.92), a very strong negative correlation with LOI (−0.95) and a strong negative correlation with Al_2O_3 (−0.81), whereas plagioclase showed very strong positive correlations with Na_2O (0.97), Fe_2O_3 (0.94) and CaO (0.93), a strong positive correlation with P_2O_5 (0.88) and a strong negative correlation with MgO (−0.71).

Scanning electron microscopy
Mixed polygonal/cylindrical tubular halloysite crystals with estimated sizes close to 3 μm long and 0.3 μm in diameter were identified in all of the samples from the Exposição pegmatite as well as in the Sigma standard sample (Fig. 7). Platy crystals of kaolinite
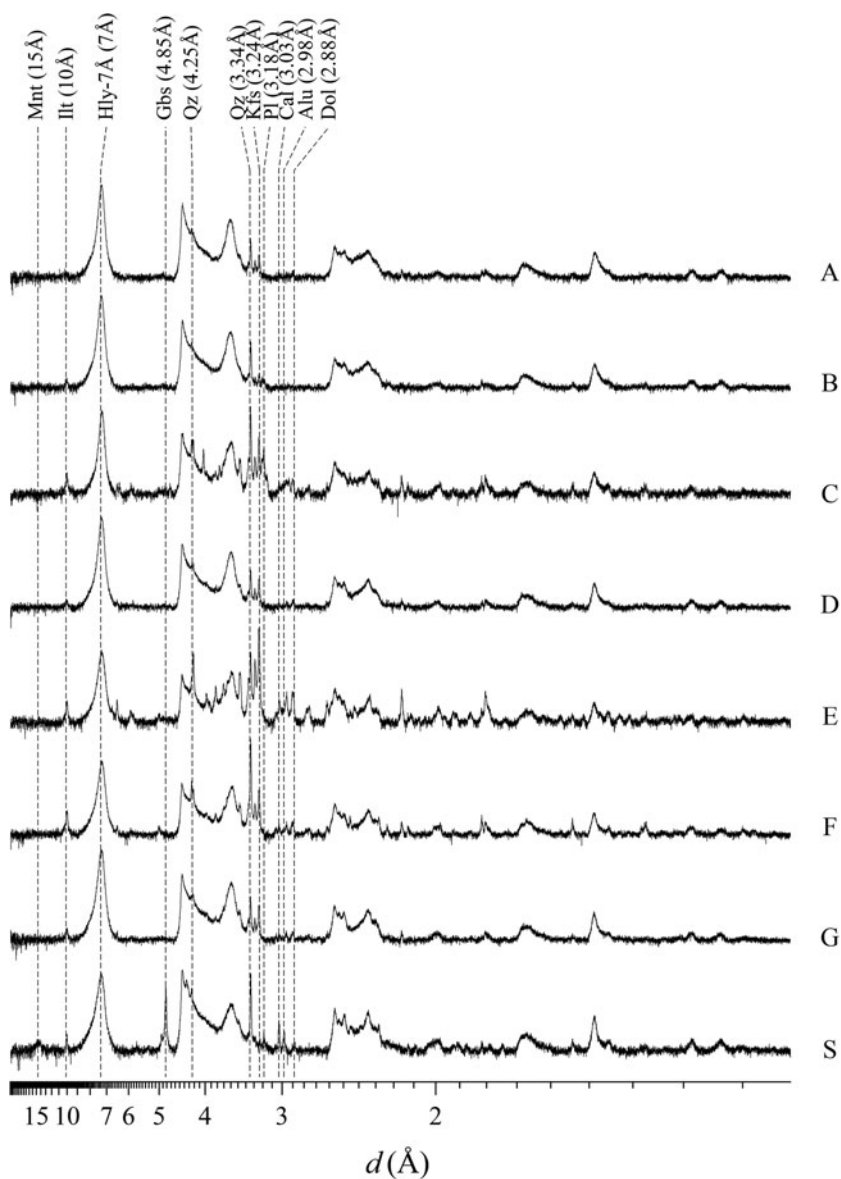
Fig. 6. XRD traces (background subtracted) of the clay fractions used in the quantitative mineral analyses by the Rietveld method. The square root scale is used for the y-axis and the diffraction traces are normalized by maximum intensity. The unprocessed data can be found in the Supplementary Materials. Hly-7Å = halloysite-7Å; Ilt = illite; Kfs = K-feldspar; Mnt = montmorillonite; Pl = plagioclase; Qz = quartz.

were observed in samples C and E with estimated sizes close to 4.5 μm long and 3.0 μm wide (Fig. 7b).

FTIR spectroscopy

Halloysite was determined by bands at 3695 and 3620 cm^{-1}, which are associated with Al–OH–Al groups (Fig. 8). The lower intensity of the 3695 cm^{-1} band in relation to the 3620 cm^{-1} band indicates hydrogen bonds between OH and H_2O in the interlayer space of halloysite (Joussein *et al.*, 2005; Madejová *et al.*, 2017). A 3600 cm^{-1} band related to structural Fe^{3+} in the octahedral sites was not identified, indicating that there is little of this metallic cation in the structure of the halloysite.

Elongated bands at 1116–1007 cm^{-1} were identified and are associated with Si–O groups, while the bands at 912 cm^{-1} mark OH-group deformations. Long bands at 533 cm^{-1} were assigned to Si–O–Al linkages, while bands at 793 and 430 cm^{-1} are interpreted as Fe–OH–Fe and Si–O–Si bands, respectively (Erkoyun & Kadir, 2011).

Particle-size distribution

Particle-size distribution analyses were performed in order to assess the efficiency of the classification by suspension (<2 μm) following Stokes' law, and to compare them with the Sigma standard sample. The results from the particle-size analysis are shown in Fig. 9. The graphs of the samples from Exposição pegmatite are unimodal with peak centre values ranging from 0.955 to 1.096 μm, minimum values ranging from 0.240 to 0.316 μm and maximum values ranging from 3.311 to 4.365 μm (Table 5). Concerning the Sigma standard sample (S), the graph showed a much broader unimodal distribution, with a peak centre at 1.660 μm and minimum and maximum particle-size values of 0.209 and 11.482 μm, respectively.
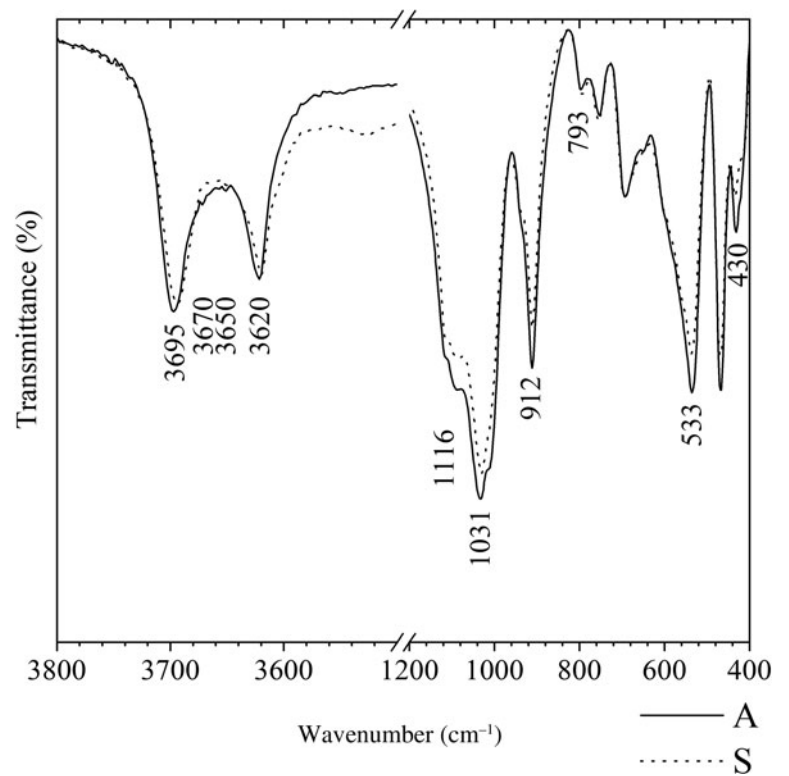
The volume of <2 μm particles in the samples from Exposição pegmatite ranged from 84.29 to 86.66 vol.%, while in the Sigma standard sample the volume of <2 μm particles was 66.35 vol.%.
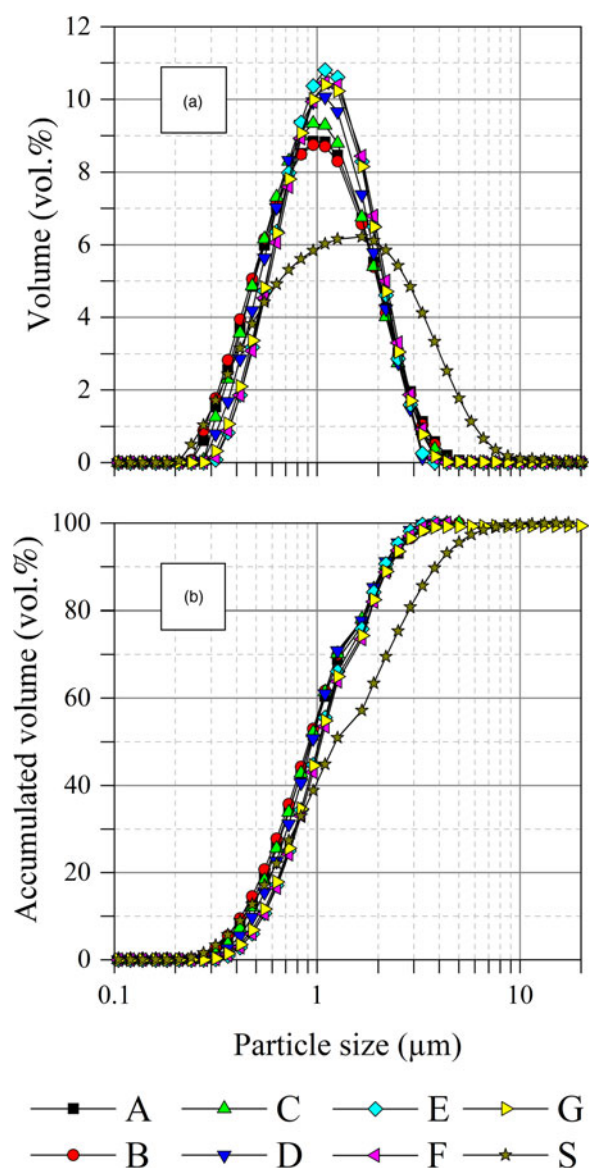
Nitrogen physisorption and CEC

The isotherms were classified as type IV according to Sing (1982), which is typical of mesoporous solids, with hysteresis type H1,
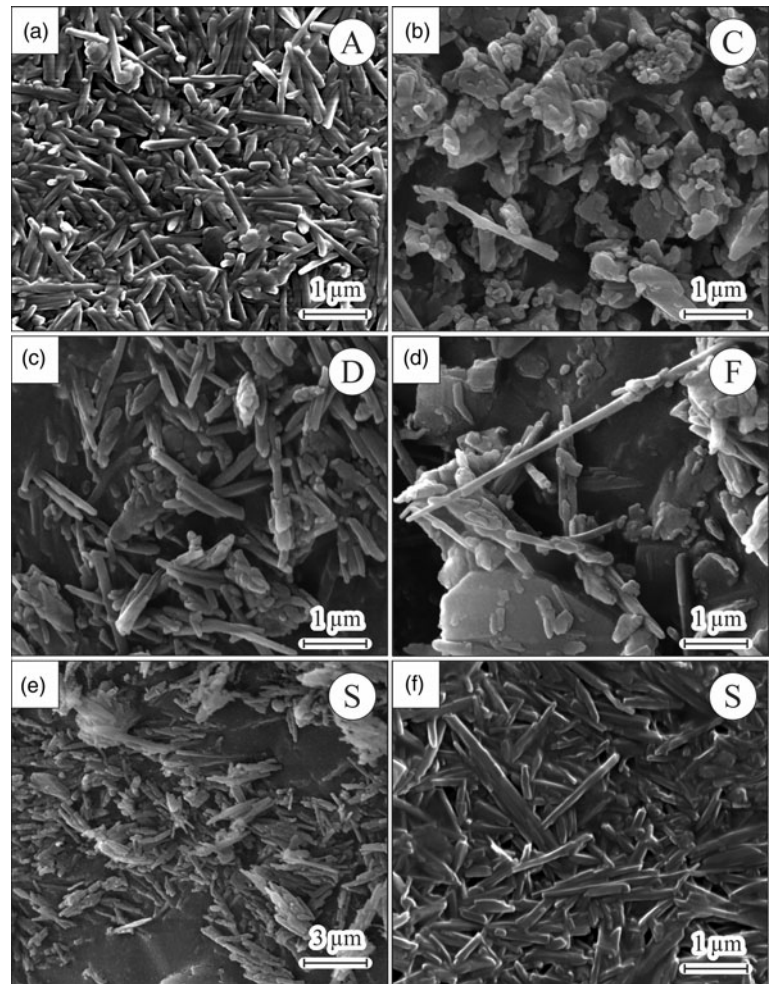
Fig. 7. SEM images of the clay fractions from the Exposição pegmatite. (a) Tubular halloysite cluster in sample A. (b) Tubular halloysite associated with platy kaolinite in sample C. (c) Tubular halloysite in sample D. (d) 6 μm-long tubular halloysite in sample F. (e & f) Tubular halloysite in the standard sample (S).

Fig. 8. Representative FTIR spectra of sample A from the Exposição pegmatite and the standard sample (S). The unprocessed data for all samples can be found in the Supplementary Materials.

Fig. 9. Particle-size distribution of the clay fractions from Exposição pegmatite and the standard sample (S). (a) Particle-size distribution (vol.%). (b) Accumulated particle-size distribution (vol.%).

Table 5. Values obtained from the particle-size distribution of the clay fractions from Exposição pegmatite and the standard sample.

Sample	Peak centre (μm)	Min. (μm)	Max. (μm)	<2 μm (vol.%)
A	0.955	0.240	4.365	85.14
B	0.955	0.240	4.365	85.82
C	0.955	0.275	4.365	86.66
D	1.096	0.275	3.311	87.30
E	1.096	0.316	3.311	86.29
F	1.096	0.316	3.802	84.29
G	1.096	0.275	3.802	84.60
Standard	1.660	0.209	11.482	65.35

Max. = maximum particle size; Min. = minimum particle size.

standard samples were 0.009 and 0.039 cm^3 g^{-1}. The CEC ranged from 4.00 (sample C) to 7.75 (sample B) cmol(+) kg^{-1}, while the Sigma standard sample CEC was 11.75 cmol(+) kg^{-1}.
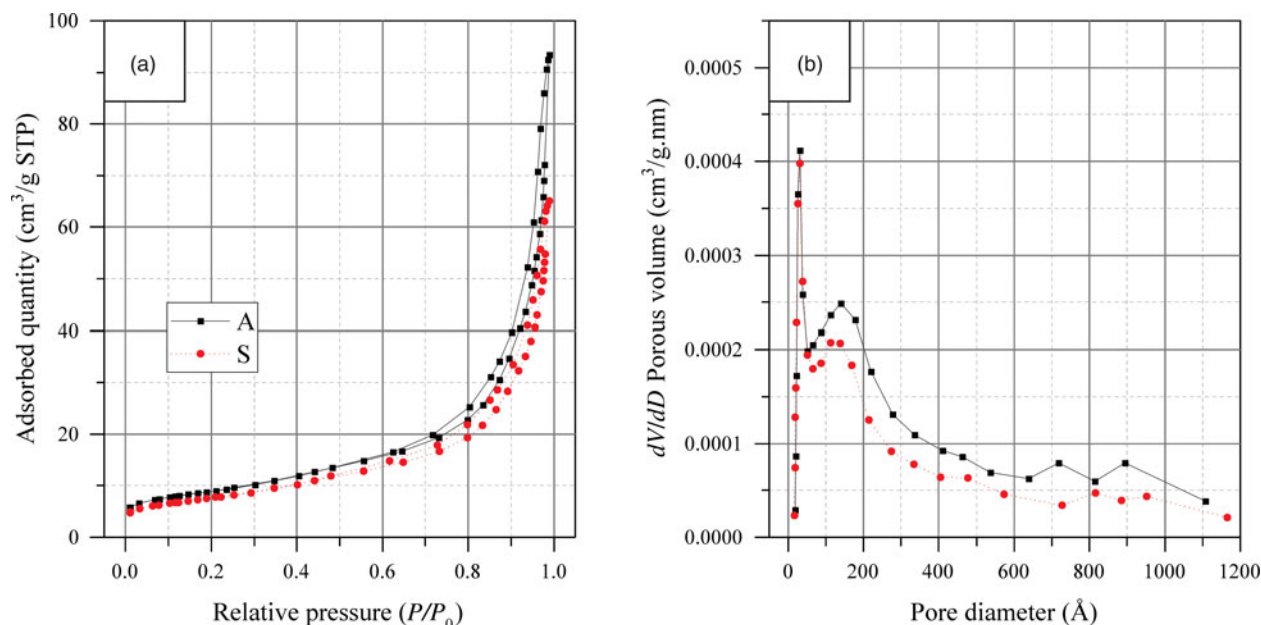
Discussion

The Exposição halloysite-rich pegmatite deposit was compared, based on its mineralogical, chemical and technologically relevant properties, with the Sigma standard sample supplied by Sigma-Aldrich. These results are discussed in the context of the well-known halloysite deposits of the Campo Alegre deposit (Brazil) (Oliveira *et al.*, 2007), the Dragon Mine deposit (USA), the Matauri Bay deposit (New Zealand) (Hillier *et al.*, 2016; Wilson & Keeling, 2016) and the regolith-hosted *REE* deposits in Zudong (China) (Li & Zhou, 2020) (Table 7).

The amount of halloysite in the bulk and the clay fractions was considered for mineral-resource estimations. After suitable processing, the halloysite may be concentrated (to ∼80%) to improve its quality. However, it is not possible to separate halloysite from other clay mineral phases, although separation from quartz, feldspar and other rock-forming minerals can be achieved. It is therefore very important to consider the abundance of halloysite in the clay mineral assemblage after excluding the non-clay minerals.

The average halloysite content in bulk samples from the Exposição deposit (25.00%) is less than that of the Campo Alegre deposit (54.03%), while the halloysite content in the clay fraction (78.5%) is close to that observed in the Sigma-Aldrich standard (83.8%), but still less than those observed in the Dragon Mine (95.9%) and Matauri Bay (90.3%) deposits. The halloysite comprises 91.8% of the clay mineral assemblage from the Exposição deposit, which is close to the grade of the Sigma-Aldrich standard (94.2%), greater than those of the Campo Alegre (60.3%) (Oliveira *et al.*, 2007) and Zudong (23.5%) deposits (Li & Zhou, 2020), and very close to those of the Dragon Mine (96.4%) and Matauri Bay (99.1%) deposits (Hillier *et al.*, 2016; Wilson & Keeling, 2016).

The clay fractions from the Exposição pegmatite showed improved technological properties (high halloysite contents, suitable particle size, micromorphological features) compared to those observed in Zudong, and these were similar to those reposed in the Sigma-Aldrich sample and from the Matauri Bay deposit. However, these properties are inferior compared to the deposit at Dragon Mine. This can probably be ascribed to the halloysite morphology, as the Dragon Mine deposit contains a high proportion of cylindrical halloysite (Hillier *et al.*, 2016) compared to the mixed polygonal/cylindrical morphologies of the Exposição

indicating a cylindrical porous morphology that was associated with the lumen region of halloysite (Fig. 10). The porosity diagram displays a bimodal distribution with peaks at 3.1 nm, which is associated with internal and/or surface porosity, and close to 14.1 nm, which is related to the lumen region of halloysite; for the Sigma standard sample these values were 3.1 and 11.4 nm, respectively.

The surface areas of the clay fractions from Exposição pegmatite were between 20 (sample C) and 33 (sample A) m^2 g^{-1} (Table 6); the Sigma standard sample showed a surface area value of 27 m^2 g^{-1}. The porous volume ranged from 0.083 (sample E) to 0.143 (sample A) cm^3 g^{-1}. Values between 0.005 and 0.009 cm^3 g^{-1} are related to internal and/or surface porosity, while values between 0.028 and 0.050 cm^3 g^{-1} are associated with the lumen porosity of the halloysite. The values found for the Sigma

Fig. 10. Representative results of the nitrogen physisorption. (a) Isotherms of samples A and the standard sample (S). (b) Porosity distribution following BJH method of sample A and the standard sample (S). STP = standard temperature and pressure.

Table 6. Technological properties obtained from the nitrogen physisorption and CEC of the clay fractions.

Sample	SA_{BET} (m^2 g^{-1})	P_m (0–5 nm)	P_m (5–30 nm)	V_p (cm^3 g^{-1})	V_p (0–5 nm) (cm^3 g^{-1})	V_p (5–30 nm) (cm^3 g^{-1})	CEC (cmol(+) kg^{-1})
A	31	3.1	14.1	0.143	0.009	0.050	7.25
B	33	3.1	11.4	0.141	0.009	0.049	7.75
C	20	3.1	13.9	0.096	0.005	0.032	4.00
D	30	3.1	13.8	0.124	0.008	0.045	7.50
E	20	3.1	13.9	0.083	0.005	0.028	4.75
F	26	3.1	13.9	0.114	0.007	0.038	7.25
G	27	3.1	13.8	0.100	0.008	0.040	7.75
Standard	27	3.1	11.4	0.100	0.009	0.039	11.75

P_m = average porosity; SA_{BET} = surface area; V_p = pore volume.

deposit. A notable feature of the Exposição halloysite deposit is that it is not as enriched in *HREEs* as the Zudong deposits. These deposits originated from the weathering of A-type granites enriched in *HREEs* by hydrothermal remobilization (Li *et al.*, 2019). The Exposição pegmatite did not produce regolith-hosted *HREE* deposits like the Zudong deposits probably due to its *HREE*-poor host-rock composition.

Conclusions

Mixed polygonal/cylindrical tubular halloysite-7Å with estimated sizes close to 3.0 µm in length and 0.3 µm in diameter was identified in the Exposição pegmatite with abundances ranging from 6.3% to 35.4%. The average chemical composition of the clay fractions was 45.46 wt.% SiO_2, 36.10 wt.% Al_2O_3, 14.62 wt.% LOI and 1.04 wt.% Fe_2O_3. The clay fractions from the Exposição halloysite deposit

presented technological properties (large halloysite contents, suitable particle size, micromorphological features) that were similar to those of world-class halloysite deposits, such as Dragon Mine (USA) and Matauri Bay (New Zealand). However, no *REE* mineralization, as in the Zudong deposits (China), were reported.

The average halloysite grade in the clay fractions of the Exposição pegmatite (78.5%) is as high as other world-class halloysite deposits, such as Dragon Mine (USA) (95.9%) or Matauri Bay (New Zealand) (90.3%), and it was greater than that of other halloysite deposits such as Campo Alegre (Brazil) and Zudong (China). The grade of the processed Exposição deposit is also close to the 83.8% purity of the halloysite standard supplied by Sigma-Aldrich.

Supplementary material. To view supplementary material for this article, please visit https://doi.org/10.1180/clm.2021.8

Table 7. Comparison of the mineralogical, chemical and technological properties of the Exposição halloysite deposit, the Sigma-Aldrich sample, the Campo Alegre deposit in Santa Catarina (Brazil), the Dragon Mine deposit (USA), the Matauri Bay deposit (New Zealand) and the Zudong deposit (China). The values are expressed from the minimum to the maximum with the average in parentheses.

Deposit/reference	Exposição, Rio de Janeiro (Brazil), this paper ($n = 7$)	Sigma-Aldrich 685445 ($n = 1$)	Campo Alegre (Brazil), Oliveira et al. (2007) ($n = 25$)	Dragon mine (USA), Hillier et al. (2016), Wilson & Keeling (2016) ($n = 15$)	Matauri Bay (New Zealand), Hillier et al. (2016), Wilson & Keeling (2016) ($n = 4$)	Zudong (China), Li & Zhou (2020) ($n = 12$)
Mineralogy						
Halloysite (wt.%) (bulk sample)	6.3–35.4 (25.0)	–	2.1–90.8 (54.0)	–	–	–
Halloysite (wt.%) (clay fraction)	58.0–89.8 (78.5)	83.8	–	80.5–100 (95.9)	86.0–98.8 (90.3)	–
Halloysite (wt.%) (clay mineral assemblage)	87.0–94.4 (91.8)	94.2	2.1–92.3 (60.3)	80.5–100 (96.4)	97.8–100 (99.1)	2.0–36.0 (23.5)
Chemical assay (wt.%) (clay fraction)						
SiO_2	42.80–51.00 (45.46)	36.70	45.05–75.22 (58.08)	44.61–46.45 (45.73)	47.24–50.13 (48.52)	–
Al_2O_3	31.00–39.30 (36.10)	38.00	15.80–37.74 (27.63)	37.55–39.93 (38.88)	35.52–38.20 (37.05)	–
LOI	11.20–16.00 (14.62)	21.10	8.05–16.75 (12.19)	13.92–16.15 (14.54)	13.95–13.97 (13.96)	–
Fe_2O_3	0.67–2.20 (1.04)	0.67	0.19–3.15 (0.90)	0.00–2.52 (0.36)	0.25–0.40 (0.29)	–
TiO_2	–	–	0.01–0.51 (0.24)	0.00–0.01 (0.02)	0.07–0.10 (0.08)	–
Others	1.47–5.68 (2.84)	3.64	0.11–6.96 (0.96)	0.09–2.10 (0.35)	0.07–0.09 (0.08)	–
Technological properties (clay fraction)						
SA_{BET} ($m^2 g^{-1}$)	20–33 (27)	27	–	30–76 (53)	23–35 (28)	8–18 (15)
V_p ($cm^3 g^{-1}$)	0.083–0.143 (0.114)	0.100	–	0.130–0.250 (0.184)	0.080–0.160 (0.120)	0.060–0.120 (0.098)
CEC ($cmol(+) kg^{-1}$)	4.00–7.75 (6.61)	11.75	5.6–11.2 (9.0)	4.90–6.30 (5.50)	2.00–3.40 (2.50)	13.0–16.6 (15.0)
ΣREE (ppm)	14.59–116.02 (44.95)	95.97	–	–	–	406–4545 (2293)

SA_{BET} = surface area; V_p = pore volume.

References

Angeleri F.B., Souza Santos P. & Souza Santos H. (1963) Características físico-químicos e cerâmicos de caulins e argilas usados na Indústria Cerâmica de S. Paulo. VII – Caulins creme amarelados de Parelheiros, Estado de S. Paulo. *Cerâmica*, **9**, 19.

ASTM C837-09 (2009) *Standard Test Method for Methylene Blue Index of Clay*. ASTM International, Wast Coshohocken, PA, USA.

Azevedo A.M.V. & Souza Santos P. (1975) Estudo da utilização do acetato de potássio na identificação de caulinita e haloisita em caulins brasileiros. *Cerâmica*, **21**, 191–206.

Barrett E.P., Joyner L.G. & Halenda P.P. (1951) The determination of pore volume and area distributions in porous substances. I. Computations from nitrogen isotherms. *Journal of the American Chemical Society*, **73**, 373–380.

Brathwaite R.L., Christie A.B., Faure K., Townsend M.G. & Terlesk, S. (2012) Origin of the Matauri Bay halloysite deposit, Northland, New Zealand. *Mineralium Deposita*, **47**, 897–910.

Brigatti M.F., Guidotti C.V., Malferrari D. & Sassi, F.P. (2008) Single-crystal X-ray studies of trioctahedral micas coexisting with dioctahedral micas in metamorphic sequences from western Maine. *American Mineralogist*, **93**, 396–408.

Brindley G.W. & Brown G. (editors) (1980) *Crystal Structure of Clay Minerals and Their X-Ray Identification*. Mineralogical Society, London, UK, 504 pp.

Brunauer S., Emmett P.H. & Teller E. (1938) Adsorption of gases in multimolecular layers. *Journal of the American Chemical Society*, **60**, 309–319.

Campos T.W. & Souza Santos H. (1986) Estudo de caulins brasileiros por microscopia eletrônica de transmissão. *Cerâmica*, **32**, 355–360.

Cheary R.W. & Coelho A. (1992) A fundamental parameters approach to X-ray line-profile fitting. *Journal of Applied Crystallography*, **25**, 109–121.

Churchman G.J., Pasbakhsh P. & Hillier S. (2016) The rise and rise of halloysite. *Clay Minerals*, **51**, 303–308.

Churchman G.J., Whitto, J.S., Claridge G.G.C. & Theng, B.K.G. (1984) Intercalation method using formamide for differentiating halloysite from kaolinite. *Clays and Clay Minerals*, **32**, 241–248.

Dill H.G., Dohrmann R., Kaufhold S. & Balaban S. (2015) Kaolinization – a tool to unravel the formation and unroofing of the Pleystain pegmatite–aplite system (SE Germany). *Ore Geology Reviews*, **69**, 33–56.

Drits V.A., Sakharov B.A. & Hillier S. (2018) Phase and structural features of tubular halloysite (7 Å). *Clay Minerals*, **53**, 691–720.

Ece Ö.I., Schroeder P.A., Smilley M.J. & Wampler J.M. (2008). Acid-sulphate hydrothermal alteration of andesitic tuffs and genesis of halloysite and alunite deposits in the Biga Peninsula, Turkey. *Clay Minerals*, **43**, 281–315.

Erkoyun H. & Kadir S. (2011) Mineralogy, micromorphology, geochemistry and genesis of a hydrothermal kaolinite deposit and altered Miocene host volcanites in the Hallaçlar area, Uşak, western Turkey. *Clay Minerals*, **46**, 421–448.

Fentaw H.M. & Mengistu T. (1998) Comparison of Kombelcha and Bombowha kaolins of Ethiopia. *Applied Clay Science*, **13**, 149–164.

Goodyear J. & Duffin W.J. (1961) An X-ray examination of an exceptionally well crystallized kaolinite. *Mineralogical Magazine and Journal of the Mineralogical Society*, **32**, 902–907.

Guggenheim S., Adams J.M., Bain D.C., Bergaya F., Brigatti M.F., Drits V.A. et al. (2006) Summary of recommendations of nomenclature committees

relevant to clay mineralogy: report of the Association Internationale pour l'Etude des Argiles (AIPEA) Nomenclature Committee for 2006. *Clays and Clay Minerals*, **54**, 761–772.

Heilbron M., Eirado L.G. & Almeida J.C.H. (2016) *Mapa geológico e de recursos minerais do Estado do Rio de Janeiro*. 1 map: 80 cm × 120 cm. Scale 1:400,000. Programa Geologia do brasil (PGB), Mapas Geológicos Estaduais. CPRM – Serviço Geológico do Brasil, Superintendência Regional de Belo Horizonte, Belo Horizonte, Brazil.

Hillier S., Brydson R., Delbos E., Fraser T., Gray N., Pendlowski H. *et al.* (2016) Correlations among the mineralogical and physical properties of halloysite nanotubes (HNTs). *Clay Minerals*, **51**, 325–350.

Joussein E., Petit S., Churchman J., Theng B., Righi D. & Delvaux B. (2005) Halloysite clay minerals – a review. *Clay Minerals*, **40**, 383–426.

Kern A. & Eysel W. (1993) *ICDD Grant-in-Aid 1993*. Mineralogische-Petrographisches Institut, University of Heidelberg, Heidelberg, Germany.

Kildale M.B. & Thomas R.C. (1957) *Geology of the Halloysite Deposit at the Dragon Mine*. Technical report. Utah Geological Association, Salt Lake City, UT, USA.

Li M.Y.H. & Zhou M.F. (2020) The role of clay minerals in formation of the regolith-hosted heavy rare earth element deposits. *American Mineralogist*, **105**, 92–108.

Li M.Y.H., Zhou M.F. & Williams-Jones A.E. (2019) The genesis of regolith-hosted heavy rare earth element deposits: insights from the world-class Zudong deposit in Jiangxi Province, South China. *Economic Geology*, **114**, 541–568.

Madejová J., Gates W.P. & Petit S. (2017) IR spectra of clay minerals. Pp. 107–149 in: *Developments in Clay Science 8: Infrared and Raman Spectroscopies of Clay Minerals* (W.P. Gates, J.T. Kloprogge, J. Madejová & F. Bergaya, editors). Elsevier, Amsterdam, The Netherlands.

Menezes S.O. (1982) *Catálogo dos principais pegmatitos do Estado do Rio de Janeiro*. DRM-RJ, Niterói, Brazil, 134 pp.

Menezes S.O. (1997) Principais Pegmatitos do Estado do Rio de Janeiro. Pp. 405–414 in: *Principais depósitos minerais do brasil* (C. Schobbenhaus, E.T. Queiroz & C.E.S. Coelho, editors). DNPM/CPRM, Brasilia, Brazil.

Montes C.R., Melfi A.J., Carvalho A., Vieira-Coelho A.C. & Formoso, M.L. (2002). Genesis, mineralogy and geochemistry of kaolin deposits of the Jari River, Amapá State, Brazil. *Clays and Clay Minerals*, **50**, 494–503.

Moore D.M. & Reynolds R.C. Jr (1989). *X-Ray Diffraction and the Identification and Analysis of Clay Minerals*. Oxford University Press, Oxford, UK, 332 pp.

Morris H.T. (1964) *Geology of the Eureka Quadrangle Utah and Juab Counties, Utah. Geological Survey Global Tubular Halloysite Deposits 323: Bulletin 1142-K*. United States Government Printing Office, Washington, DC, USA, 29 pp.

Morris H.T. (1985) Geology, ore bodies and halloysite deposits of the Tintic Mining District. Presented at: *International Clay Conference*, Denver, CO, USA.

Oliveira M.T., Furtado S., Formoso M.L., Eggleton R.A. & Dani N. (2007) Coexistence of halloysite and kaolinite: a study on the genesis of kaolin clays of Campo Alegre Basin, Santa Catarina State, Brazil. *Anais da Academia Brasileira de Ciências*, **79**, 665–681.

Oliveira M.T.G., Petit S., Grauby O., Formoso M.L.L. & Trescases J.J. (1997) Characterization and distribution of halloysitic clay minerals in weathered basalts (Southern Paraná Basin, Brazil). *Anais da Academia Brasileira de Ciências*, **69**, 179–192.

Paiva N.J.E. (1956) Características de alguns caulins dos arredores da cidade de São Paulo. *Cerâmica*, **2**, 111–144.

Parker J.M. III (1946) *Residual Kaolin Deposits of the Spruce Pine District, North Carolina*. Technical report. United States Geological Survey, Raleigh, NC, USA, 45 pp.

Pimentel A.C. (1966) Distribuição geográfica de caulins cauliníticos e haloysíticos do Brasil. *Cerâmica*, **12**, 161–172.

Prasad M.S., Reid K.J. & Murray H.H. (1991) Kaolin: processing, properties and applications. *Applied Clay Science*, **6**, 87–119.

Saddiqui M.A. & Ahmed Z. (2005) Mineralogy of the Swat kaolin deposits, Pakistan. *Arabian Journal for Science and Engineering*, **30**, 195–218.

Salgado-Campos V.M.J., Bertolino L.C. & Alves O.C. (2017) Mineralogical characterization and beneficiation study of kaolin from Equador (RN)

and Junco do Seridó (PB) to increase the brightness index. *Cerâmica*, **63**, 369–375.

Salgado-Campos V.M.J., Bertolino L.C., Nascimento L.C.S., Leite J.Y.P., Brandão V.S., Alves O.C. & Tolentino J. Jr (2019) Mineralogy and technological characterization of two kaolin deposits from the Borborema Pegmatite Province, northeastern Brazil. *Clay Minerals*, **54**, 283–291.

Salgado-Campos V.M.J., Bertolino L.C., Silva F.J. & Mendes J.C. (2020) Mineralogical characterization of clay mineral assemblages from Rio de Janeiro pegmatites to identify kaolinite and/or halloysite deposits. *Cerâmica*, **66**, 483–495.

Santos H.A.B.J. (2017) *Caracterização mineralógica do caulim proveniente de pegmatitos da região de Rio Bonito – RJ visando a identificação de halloysita*. Departamento de Geociências, Instituto de Agronomia, Universidade Federal Rural do Rio de Janeiro, Trabalho de Conclusão de Curso, Rio de Janeiro, Brazil, 68 pp.

Santos H.N., Neumann R. & Ávilla C.A. (2017) Mineral quantification with simultaneous refinement of Ca-Mg carbonates non-stoichiometry by X-ray diffraction, Rietveld method. *Minerals*, **7**, 164.

Schukow H., Breitinger D.K., Zeiske T., Kubanek F., Mohr J. & Schwab R.G. (1999) Localization of hydrogen and content of oxonium cations in alunite *via* neutron diffraction. *Zeitschrift für anorganische und allgemeine Chemie*, **625**, 1047–1050.

Silva M.R.R. & Dantas J.R.A. (1997) Província pegmatítica da Borborema Seridó, Paraíba e Rio Grande do Norte. Pp. 441–467 in: *Principais Depósitos Minerais do Brasil*, 1 ed., v. 4b. DNPM/CPRM, Brasília, Brazil.

Sing K.S.W. (1982) Reporting physisorption data for gas/solid systems. *Pure and Applied Chemistry*, **54**, 2201–2218.

Sousa D.J.L.D., Varajão A.F.D.C., Yvon J. & Da Costa G.M. (2007) Mineralogical, micromorphological and geochemical evolution of the kaolin facies deposit from the Capim region (northern Brazil). *Clay Minerals*, **42**, 69–87.

Souza Santos P. & Pimentel A.C. (1971) Estudos sobre a presença de caulinita e haloisita em caulins brasileiros. *Cerâmica*, **17**, 258–295.

Souza Santos P., Souza Santos H.L. & Brindley G.W. (1964) Mineralogical studies of kaolinite – halloysite clays: part II. Some Brazilian kaolins. *Proceedings of the International Clay Conference*, **49**, 1543–1550.

Souza Santos P., Souza Santos H.L. & Moniz A.C. (1962) Estudos de algumas argilas e caulins de diversos Estados do Brasil. *Cerâmica*, **8**, 2–21.

Souza Santos P., Toledo S.P. & Souza Santos H. (2009) Caulins haloisíticos das Regiões Sudeste e Sul do Brasil. *Cerâmica Industrial*, **14**, 14–20

Technisch Physische Dienst (1966) *ICDD Grant-in-Aid 1966*. Technisch Physische Dienst, Delft, The Netherlands.

Technisch Physische Dienst (1967) *ICDD Grant-in-Aid 1967*. Technisch Physische Dienst, Delft, The Netherlands.

Toledo S.P., Souza Santos H. & Souza Santos P.C. (2002) Clay mineral characterization in kaolins and ball clays from Santa Catarina. *Acta Microscópica*, **11**, 1–12.

Tolentino J. Jr (2019) *Potencial dos depósitos de caulim halloysítico associados aos pegmatitos da região de Juiz de Fora visando o seu aproveitamento econômico*. PhD thesis, Programa de Pós-Graduação em Geociências, Universidade do Estado do Rio de Janeiro, Rio de Janeiro, Brazil, 165 pp.

Velde B.B. & Meunier A. (2008). *The Origin of Clay Minerals in Soils and Weathered Rocks*. Springer Science+Business Media, Berlin, Germany.

Viani A., Gualtieri A.F. & Artioli G. (2002) The nature of disorder in montmorillonite by simulation of X-ray powder patterns. *American Mineralogist*, **87**, 966–975.

Visconti Y.S. & Nicot B.N.F. (1957) Mutilização do caulim tubular. *Cerâmica*, **3**, 72–80.

Visconti Y.S., Nicot B.N.F., De Andrade E.G., Electron Micrographs & Villanova A.C. (1956) Tubular morphology of some Brazilian kaolins. *American Mineralogist*, **41**, 67–75.

Warr L.N. (2020) Recommended abbreviations for the names of clay minerals and associated phases. *Clay Minerals*, **55**, 261–264.

Weaver C.E. (1976) The nature of TiO_2 in kaolinite. *Clays and Clay Minerals*, **24**, 215–218.

Whitney D.L. & Evans B.W. (2010) Abbreviations for names of rock-forming minerals. *American Mineralogist*, **95**, 185–187.

Wilson I.R. (2004) Kaolin and halloysite deposits of China. *Clay Minerals*, **39**, 1–15.

Wilson I.R. & Keeling J. (2016) Global occurrence, geology and characteristics of tubular halloysite deposits. *Clay Minerals*, **51**, 309–324.

Wilson I.R., Santos H.D.S. & Santos P.D.S. (1998) Caulins brasileiros: alguns aspectos da geologia e da mineralogia. *Cerâmica*, **44**, 118–129.

Wilson I.R., Souza Santos H. & Souza Santos P. (2006) Kaolin and halloysite deposits of Brazil. *Clay Minerals*, **41**, 697–716.